Combustion waves in composite solid material of shell-core type

Vladimir V. Gubernov,
I.E. Tamm Theory Department, P.N. Lebedev Physical Institute,
Moscow 119991, 53 Leninskii prosp., Russian Federation,
Email: vvg@spmlab.phys.msu.su

Vadim N. Kurdyumov,
Department of Energy, CIEMAT, Avda. Complutense 40, 28040 Madrid, Spain,

Andrei V. Kolobov,
I.E. Tamm Theory Department, P.N. Lebedev Physical Institute,
Moscow 119991, 53 Leninskii prosp., Russian Federation,

December 12, 2015

Abstract

In this paper the asymptotic and numerical analysis of the combustion wave propagation in the shell-core composite solid energetic material is undertaken based on the diffusional-thermal model with an overall Arrhenius reaction step. Flame speed and structure are found for the broad range of parameter values. Two different regimes of flame propagation are identified. In the weak recuperation regime the temperature of shell and core are monotonic functions of coordinate, which differ only slightly in the reaction zone of the flame. In the strong recuperation regime the temperature of the shell is significantly higher than the temperature of the core. It has a sharp peak in the reaction zone with the maximum value exceeding the adiabatic flame temperature for pure energetic material. It is found that the highest level of flame acceleration in the composite material can be attained in the strong recuperation regime. The competition of these flame propagation regimes may lead to the coexistence of multiple combustion waves traveling with different velocities. Stability of combustion waves in practically important strong recuperation regime is investigated.

keywords: combustion waves, thermal-diffusive instabilities, composite energetic materials, flame multiplicity

1 Introduction

An increase in the burning rate and stabilization of deflagration in combustion of solid materials are important goals in a number of practical applications which include the development of propellants for solid thrust engines [1], high temperature self-propagating synthesis of advanced materials [2], design and engineering of combustion-based micro-electro mechanical systems [3]. The conventional approaches to the enhancing the burning rate are focused on increasing the flame surface or modifying the combustion chemistry as described in [1]. Recent experiments [3, 4] with mirco- and nanosized materials can offer an alternative way to address these issues.

The reported systems are mostly aimed at the mirco-thrust and micro-power generation applications [3, 4]. They consist of two key elements: the inert highly thermo-conductive unit and the reacting material, which are kept in thermal contact. The role of conducting element is to recirculate heat from the hot products to the fresh mixture i.e. a well known in gas micro combustion "excess enthalpy" principle is employed here [5]. The idea to increase the flame speed by the use of heat conducting elements was demonstrated in experiments [6]. However at that time the production of arrays of aligned wires of micro- and nanosize was technologically not achievable. This hindered the development of composite energetic material based of the heat conducting matrix.

In [7] a one-dimensional diffusional-thermal adiabatic model of composite material of shell-core type is investigated. The enthalpy feedback is provided by highly conductive core and the heat is produced by the reacting shell material. It is demonstrated that the heat recirculation in such system leads to substantial increase of normal flame speed, superadiabatic combustion and flame stabilization, which is in qualitative agreement with the effects observed in gas mirco combustion [8].

In this paper we continue to investigate the propagation of combustion waves in the shell-core composite solid propellants. We aim to systematically study the speed, structure and stability of deflagration waves in this system by means of asymptotic and numerical analysis in experimentally feasible parameter range.

2 General formulation

We consider a problem of the planar flame propagation in composite material which is an array of closely packed shell-core structures [7]. The shell-core structures are considered individually. They are constituted of similar sized highly heat conductive cylinders, which can be nanowires or nanotubes. The core element of the structure remains chemically inert. Its main function is to provide recuperation of heat from product zone to preheat zone of combustion wave. Every conductive wire is wrapped with a cylindrical shell of energetic combustible solid material of the uniform thickness. The chemical reaction is modeled by an over-all reaction step that converts solid fuel to products at mass rate proportional to Y with Arrhenius temperature dependence $\Omega = \mathcal{B}Y \exp(-E/RT_1)$, where T_1 is the temperature and Y is the mass fraction of the energetic material, E is the activation energy of the reaction, while $\mathcal{B}$ represents the frequency factor of the reaction. The boundary conditions on the outer interface of the energetic material are considered to be adiabatic. In most cases these conditions are not exactly adiabatic, since there always exist conductive and/or radiative heat losses. Nevertheless we consider an array of closely packed shell-core structures (as it is done in experiments in [3]). In this case the heat is lost from the outer surface of the array and is therefore substantially reduced for each of the shell-core structures.

The dimensional balance equations describing conservations of energy in both mediums and mass of fuel are taken from [7] as follows

$$S_1\left\{\rho_1 c_1 \frac{\partial T_1}{\partial t} + \rho_1 c_1 U_f \frac{\partial T_1}{\partial x} - \lambda_1 \frac{\partial^2 T_1}{\partial x^2} - Q\Omega\right\} = -PK(T_1 - T_2), \tag{1}$$

$$S_2\left\{\rho_2 c_2 \frac{\partial T_2}{\partial t} + \rho_2 c_2 U_f \frac{\partial T_2}{\partial x} - \lambda_2 \frac{\partial^2 T_2}{\partial x^2}\right\} = PK(T_1 - T_2), \tag{2}$$

$$S_1\left\{\rho_1 \frac{\partial Y}{\partial t} + \rho_1 U_f \frac{\partial Y}{\partial x} - \Omega\right\} = 0, \tag{3}$$

where indexes '1' and '2' refer to the solid combustible and pure conductive sections, $\rho_{1,2}$ is the density, $c_{1,2}$ is the specific heat, $T_{1,2}$ is the temperature, $\lambda_{1,2}$ - thermal conductivity, $S_{1,2}$ is the area of corresponding sections; P is the perimeter of the intermediate surface, K is an effective heat-exchange coefficient, Q is the heat of the reaction, U_f, is the combustion wave propagation speed.

The mass fraction is normalized with respect to the upstream value, Y_0, and non-dimensional temperatures, $\theta_1 = (T_1 - T_0)/(T_a - T_0)$ and $\theta_2 = (T_2 - T_0)/(T_a - T_0)$, are introduced where $T_a = T_0 + QY_0/c_1$ denotes the adiabatic flame temperature and T_0 is the ambient temperature. Let us define the characteristic time and length using the relations

$$t_c = \beta \mathcal{B}^{-1} \exp(E/RT_a), \quad l_c = \sqrt{t_c \alpha_1}, \tag{4}$$

where $\beta = \gamma E/RT_a$ is the Zel'dovich number and $\gamma = (T_a - T_0)/T_a$ is the heat release parameter. The non-dimensional governing equations become

$$\frac{\partial \theta_1}{\partial t} + u_f \frac{\partial \theta_1}{\partial x} = \frac{\partial^2 \theta_1}{\partial x^2} + \omega - \xi \cdot (\theta_1 - \theta_2), \tag{5}$$

$$\frac{\partial \theta_2}{\partial t} + u_f \frac{\partial \theta_2}{\partial x} = \alpha \frac{\partial^2 \theta_2}{\partial x^2} + s \cdot \xi \cdot (\theta_1 - \theta_2), \tag{6}$$

$$\frac{\partial Y}{\partial t} + u_f \frac{\partial Y}{\partial x} = -\omega \tag{7}$$

with $u_f = t_c U_f / l_C$ representing the dimensionless flame velocity and the dimensionless reaction rate ω given by

$$\omega = \beta Y \exp\left\{\frac{\beta(\theta_1 - 1)}{1 + \gamma(\theta_1 - 1)}\right\}. \tag{8}$$

Appropriate boundary conditions are

$$\begin{array}{ll} x \to -\infty: & \theta_1 = \theta_2 = Y - 1 = 0, \\ x \to +\infty: & \partial Y/\partial x = \partial\theta_1/\partial x = \partial\theta_2/\partial x = 0 \end{array} \tag{9}$$

far upstream and downstream.

The parameters appearing in these equations are

$$\alpha = \alpha_2/\alpha_1, \quad \xi = \frac{KP\beta \exp(E/RT_a)}{\rho_1 c_1 S_1 \mathcal{B}}, \quad s = \frac{\rho_1 c_1 S_1}{\rho_2 c_2 S_2}. \tag{10}$$

The parameter $\alpha = \alpha_2/\alpha_1$ gives the ratio of the thermal diffusivities $\alpha_1 = \lambda_1/\rho_1 c_1$ and $\alpha_2 = \lambda_2/\rho_2 c_2$. It is large number here since it is crucial to have highly conductive media in order to accelerate the combustion wave. For cyclotrimethylene trinitramine - carbon nanotubes system considered in [3] parameter α can reach the values as high as 10^4.

Parameter ξ represents the ratio of the characteristic heat exchanged through the common surface between shell and core elements to the heat released in the course of the chemical reaction in the combustible material. According to the data from [3, 9, 10] it can be of the order of 10^2 for very small shell thickness or much less than that. The case $\xi = 0$ describes the flame propagating in a pure energetic material neglecting the thermal exchange with the conductive supplement. The Zel'dovich number, β, appearing in equation (8) is usually a large number and provides that $u_f \to 1$ at $\beta \gg 1$ for $\xi = 0$ in the case of the steady flame propagation.

Parameter s contains both geometric and thermo-physical quantities. The physical meaning of s is that it is a ratio of characteristic "heat capacities" of shell and core elements. Since it is mostly governed by geometric factors it can be easily manipulated in experiments and can be either small or large number. It follows from the definitions (10) that the parameters s and ξ are independent. However they are interrelated via the thermo-physical properties of the energetic material. So that if ρ_1, c_1 or S_1 are varied, the parameters s and ξ change in such a way that $s\xi$ remains constant.

3 Travelling wave solution

We seek the solution of equations (5-9) in a form of the travelling wave propagating with constant speed without changing its shape. In this case the temperature and concentration of fuel profiles depend on coordinate only and (5-9) reduce to the system of ordinary differential equations

$$\theta_{1xx} - u_f \theta_{1x} + \omega - \xi \cdot (\theta_1 - \theta_2) = 0, \tag{11}$$

$$\alpha\theta_{2xx} - u_f \theta_{2x} + s \cdot \xi \cdot (\theta_1 - \theta_2) = 0, \tag{12}$$

$$u_f Y_x - \omega = 0. \tag{13}$$

In the downstream region the temperature of fuel and thermal conduit as well as the value of fuel leakage are not defined. Since it is assumed that there is no reaction happening for $x \to +\infty$, we require that the boundary condition (9) should be a fixed point of (11-13). This is possible if the reaction term in the downstream vanishes i.e. either $Y = 0$ or θ_b is small enough so that the Arrhenious term is negligible. The latter condition implies that the thermal conduit serves as effectively a thermostat. This case is not considered here, therefore we take $Y = 0$ for $x \to +\infty$. Also in equations (11, 12) the terms corresponding to the heat exchange between the fuel and thermal conduit should vanish. Thus we require that $\theta_1 = \theta_2 = \theta_b$ for $x \to +\infty$.

Equations (11- 13) also possess an integral $S = s\theta_{1x} + \alpha\theta_{2x} + u_f(s\theta_1 + \theta_2 + sY)$. Taking into account the boundary conditions in the upstream (9), the integral S can be evaluated as $S = su_f$. In the downstream region this gives $\theta_b = s/(1+s)$. It is seen that parameter s indicates how much heat is removed from the product zone of the energetic material to the chemically inert core.

3.1 Asymptotic of large s

If s is large then the role of the core is diminishing. Such as in the situation of very thick outer shell and very thin core. In this case the temperature of the products tends to the adiabatic flame temperature of pure energetic material i.e. $\theta_b \to 1$. As it is demonstrated below the structure and the speed of combustion wave also approaches the characteristics of adiabatic flame of the pure energetic material.

The asymptotic behavior of the flame speed for large values of s can be obtained if we assume that $s \sim \xi \sim \alpha \gg 1$, i.e these parameters are asymptotically large and are of the same order of magnitude. In this case obviously, the temperatures are $\theta_1 = \theta_2 + O(1/s)$. From the other side, equations (11)-(13) give in the leading order of the asymptotic expansion over $1/s$

$$\begin{array}{l} \theta_{1xx}(1+\alpha/s) + u_f\theta_{1x} + \omega = 0, \\ u_f Y_x - \omega = 0. \end{array} \tag{14}$$

These equations can be rewritten in a standard form for the single step reaction model of flame front propagation in solid mixture if we define new coordinate $\tilde{x} = \sqrt{1+\alpha/s}$ and flame speed $\tilde{u}_f = u_f/\sqrt{1+\alpha/s}$. For the so-defined one-step model the flame speed, $\tilde{u}_f$, tends to unity for $\beta \to \infty$ by the definition. For finite parameter values it can be calculated numerically i.g. for $\beta = 8$ and $\gamma = 0.7$ this gives 1.0209.... Now we can express the flame speed as

$$u_f = \tilde{u}_f\sqrt{1+\alpha/s}. \tag{15}$$

If α/s is small equations (14) tend to the ones describing the combustion of pure solid fuel, the distribution of temperatures $\theta_{1,2}(x)$ are monotonic functions close to each other and the flame speed approaches the adiabatic combustion speed of pure energetic component of the composite. In other words the role of heat conducting element becomes negligible.

3.2 Asymptotic of small s

If s is small the temperature of the products tends to zero. The situation is encountered in the case of very thin energetic material in comparison to the heat conducting element. This means that all the heat of the reaction is absorbed into the passive core of the composite structure which behaves effectively as a thermostat. In the limit $s \to 0$ combustion waves posses the properties of flame propagation with linear heat loss to the surroundings and the results of the matched asymptotic analysis [11] applies. The dependence of flame speed on parameters is a two-valued C-shaped function with a single turning point, which is usually associated with flammability limit caused by heat losses to the surroundings.

3.3 Asymptotic of large α and β

Here we assume α and β to be asymptotically large parameters. Firstly, we consider the reaction zone region and introduce temperature expansion

$$\theta_i = \theta_b - \beta^{-1}KU_i + \ldots, \tag{16}$$

where $i = 1,\ 2$ and $K = [1+\gamma(\theta_b - 1)]^2$. The expression under the exponent in the reaction rate term can be expanded as

$$\frac{\beta(\theta_1 - 1)}{1+\gamma(\theta_1 - 1)} = \Lambda + U_i + O(\beta^{-1}), \tag{17}$$

where $\Lambda = \beta(\theta_b - 1)/(1+\gamma(\theta_b - 1))$. Next we define the inner coordinate $\eta = x\beta e^{\Lambda}/u_{1f} = \delta x$ and parameter $Q = \alpha s^{-1}u_{1f}^{-2}Ke^{\Lambda}$ and rewrite equations (11-13) leaving the leading order terms as

$$\begin{array}{l} Ye^{-U_1} + K\xi e^{-\Lambda}(U_1 - U_2) = 0, \\ QU_{2\eta\eta} + K\xi e^{-\Lambda}(U_1 - U_2) = 0, \\ Y_\eta - Ye^{-U_1} = 0, \end{array} \tag{18}$$

where it assumed that α^{-1} is at least $O(\beta^{-1})$ or smaller. It is seen from the first equation in (18) that the difference $U_1 - U_2$ is exponentially small. If ξ and s are of the order of $O(1)$, then $\theta_b \sim O(1)$ and $\Lambda \sim -\beta$. Thus in order for the second term to be balanced by the first term $U_1 - U_2 \sim e^{\Lambda} \ll 1$. This implies that U_1 can be replaced with U_2 and (18) can be written as

$$\begin{array}{l} QU_{2\eta\eta} - Ye^{-U_2} = 0, \\ Y_\eta - Ye^{-U_2} = 0, \end{array} \tag{19}$$

The system of equations (19) has to be solved subject to boundary conditions

$$\begin{array}{ll} U_2 = Y = 0 & \text{for} \quad x \to -\infty, \\ U_{2\eta} - C_1 = Y - 1 = 0 & \text{for} \quad x \to +\infty, \end{array} \tag{20}$$

where C_1 is a constant. Equations (19) have an integral $QU_{2\eta} - Y = C_2$, where $C_2 = 0$ from the boundary conditions at $\eta \to -\infty$. This allows the system of equations (19) to be rewritten as a single equation

$$U_{2\eta\eta} - U_{2\eta} e^{-U_2} = 0. \tag{21}$$

Introducing $w \equiv U_2$ as a new independent variable and $S \equiv dU_2/dw$ as new dependent variable equation (21) can be further reduced to

$$SS_w - Se^{-w} = 0, \tag{22}$$

subject to boundary conditions

$$\begin{array}{lll} S = 0 & \text{for} \quad w \to 0 & (\text{or} \quad \eta \to -\infty), \\ S = C_1 & \text{for} \quad w \to +\infty & (\text{or} \quad \eta \to \infty), \end{array} \tag{23}$$

Nontrivial solution to (22) can be written as $S = 1 - e^{-w}$. This gives $Q = 1$ and

$$u_{1f}^2 = \alpha s^{-1}(1 + \gamma(\theta_b - 1))^2 \exp\left\{\frac{\beta(\theta_b - 1)}{1 + \gamma(\theta_b - 1)}\right\}, \tag{24}$$

where $\theta_b = s/(s+1)$ as discussed earlier.

The formula for flame speed (24) is consistent with the outer matching conditions, which as usual can be found from (11-13) after neglecting the reaction terms ω. This yields the system of linear differential equations subject to (9). It can be solved to give

$$\begin{array}{ll} \theta_1 = \theta_2 = \theta_b, \ Y = 0 & \text{for} \quad x < 0, \\ \theta_1 = \theta_2 = \theta_b e^{\mu_0 x}, \ Y = e^{\mu_0 x}, & \text{for} \quad x > 0. \end{array} \tag{25}$$

where μ_0 is a largest negative root of characteristic equation

$$E(\mu) = \mu^3 + u_{1f}\mu^2(1 + \alpha^{-1}) + \mu(\alpha^{-1}(u_{1f}^2 - s\xi) - \xi) - u_{1f}\alpha^{-1}(s+1)\xi = 0. \tag{26}$$

If α is considered to be large, then in the leading order the roots of equation are $\mu_0 = 0$, $\mu_{1,2} = -1/2c \pm \sqrt{c^2 - 4\xi}/2$. The first correction with respect to α^{-1} to the vanishing root can be expressed as $\mu_0 = -u_{1f}\alpha^{-1}(s+1) + O(\alpha^{-2})$. Taking into account the above definitions the jump of derivative of the temperature across the reaction zone can be expressed as

$$\left[\frac{dU}{d\eta}\right]_-^+ = -\frac{1}{K\delta}\left[\frac{d\theta}{dx}\right]_-^+ = -\frac{\theta_b \mu_0}{K\delta}. \tag{27}$$

The inner region solution gives $[dU/d\eta]_-^+ = 1$. On the other hand substitution of the parameters into the left hand side of (27) gives the same result. Therefore the solutions to the outer and inner problems are consistent as long as

$$\beta \gg 1, \ s \sim O(1), \ \xi \geq O(1), \alpha^{-1} \leq O(\beta^{-1}). \tag{28}$$

The flame propagation regime considered here is characterized by only weak heat recuperation since the temperature distribution in shell and core elements of the composite structure are close to each other.

4 Numerical results

In order to obtain the travelling wave solutions we solve (11-13) numerically using standard shooting-relaxation algorithms. Their linear stability is investigated by using the Evans function method [12] implemented as described in [13]. The non-stationary solutions are obtained by direct integration of the partial differential equations (5-9), which are solved by the method of splitting with respect to the physical processes. Initially we solve the set of ordinary differential equations which describe temperature and fuel concentration variations due to the reaction by using the fourth order Runge-Kutta algorithm. As a next step, equations of heat and mass transfer are solved with the Crank-Nicholson method of the second-order approximation in space and time.

4.1 Speed and structure of combustion wave

In this section the results of numerical calculations of the flame speed and structure are presented. In figure 1 the dependence of u_f on α is plotted for $\beta = 8$, $\gamma = 0.7$ and different values of ξ and s, which are chosen to cover broad parameter range. Parameter α is the ratio of the thermal diffusivities of core and shell elements of energetic material. According to the results of asymptotic analysis α should be large in order to obtain $u_f > 1$ and the condition $u_f \sim 1$ corresponds to deflagration wave in pure energetic material. The asymptotic behaviour of $u_f(\alpha)$ for large α predicted by both equations (15) and (24) is proportional to $\sqrt{\alpha}$.

The results of numerical calculation are shown in figure 1 with the solid curves. The line marked as '1' shows the dependence $u_f(\alpha)$ for $\xi = 10^2$ and $s = 5$. These values of parameters satisfy the conditions (28) for applicability of flame speed estimation (24), which is also plotted in figure 1 with the dashed line. It is seen that asymptotic and numerical results agree well in the whole range of α variation from 10 to 3000 considered here. The curve '2' corresponds to the parameter values $\xi = 10^2$ and $s = 10^2$. This choice of parameters meets the conditions of applicability of equation (15). The function (15) is depicted in figure 1 with the dashed-dotted line and is also in good agreement with the numerical data. The other two asymptotic limits discussed in the previous section are $\xi \to 0$ and $s \to 0$. In the first case, $\xi \to 0$, the equations (11) reduce to the system for single step adiabatic reaction model for pure energetic material and $u_f \sim 1$. The numerical results for small nevertheless finite value of $\xi = 10^{-2}$ and $s = 5$ are shown in figure 1 with the curve '3'. The flame speed u_f weakly depends on α and does not follow the root-type behaviour. In the case $s \to 0$ the model (11) tends to the nonadiabatic one-step reaction model. Thus it is expected that u_f weakly depends on α and decays with the reduction of parameter s. The curve '4' shows the numerical data for $s = 0.4$ and $\xi = 1$. It is seen that the value of u_f significantly decreases and attains the maximum 0.145 for $\alpha = 3 \times 10^3$. From the practical point of view the regimes with $\xi \to 0$ or $s \to 0$ are not interesting since they do not allow to reach flame velocities significantly larger than $u_f = 1$.

In all asymptotic limits discussed in section 3 there is a good qualitative agreement between asymptotic and numerical results. However, for intermediate parameter values the behaviour different from predicted by equations (15) and (24) can be found. In figure 2 the dependence of the combustion wave speed on s is shown for $\alpha = 10^2$, $\beta = 8$, $\gamma = 0.7$ and two values of $\xi = 1$ and 10^2. The solid lines represent the numerical results, whereas the dash-dotted and the dotted lines are plotted according to the equations (15) and (24), respectively. For $\xi = 10^2$ the combustion wave velocity is properly described by two asymptotic results i.e. equation (15) for $s \gg 1$ and equation (24) for $s \leq 1$. The function $u_f(s)$ is single valued in this case. However as ξ is reduced to 1 the behaviour of $u_f(s)$ changes. Two fold bifurcations emerge and there exists a region of values of s with triple coexisting solutions travelling with different velocities i.e. fast, slow and intermediate solution branches. In some sense this situation resembles the multiplicity of combustion wave solutions in the model with two stage competing reactions [14], which is chemistry driven and is caused by the presence of two parallel reaction paths. Mathematically the system of equations (5–7) is also a set of three partial differential equations as in [14], however in current model there is only single reaction pathway nevertheless multiplicity is possible even in such situation.

There are two points $s = 4$ and $s = 1.2$ in figure 2 located on the fast and slow solution branches of $u_f(s)$ for the case of $\xi = 1$, which are numbered as '1' and '2', respectively. We sample two solution profiles for this specific parameter values. The solution profile on the fast branch is demonstrated in figure 3, where the dependence of temperature of the reacting shell, Θ_1, temperature of inert core, Θ_2, and mass fraction of fuel, Y, on coordinate, x, in the co-moving frame are plotted with the solid, the dashed and the dash-dotted lines, respectively. The coordinate is scaled so as to cover the range from 0 to 1. The length of the interval of integration $x \in [0, L]$ is $L \approx 37.7$. It is clearly seen that there is a strong recuperation effect in this regime of flame propagation. Heat is effectively absorbed from the product region, where $\Theta_1 > \Theta_2$, and transfered via the highly conductive core to the preheat region, where Θ_2 significantly exceeds Θ_1. The maximum temperature of the reacting shell reaches values as large as 1.2. The adiabatic burned temperature for pure energetic material is equal to 1 in our scaling. Thus the composite material burn at the superadiabatic temperature in this regime, which we call the strong recuperation regime.

The profiles $\Theta_1(x)$, $\Theta_2(x)$ and $Y(x)$ are plotted in figure 4 with the solid, the dashed and the dash-dotted lines, respectively. The choice of parameter values $\alpha = 10^2$, $\beta = 8$, $\gamma = 0.7$, $\xi = 4$ and $s = 1.6$ corresponds to the point '2' in figure 2, which is located on the slow solution branch of $u_f(s)$ dependence. The coordinate is scaled so as to cover the range from 0 to 1. The length of the interval of integration $x \in [0, L]$ is $L \approx 203.3$. We call this regime of deflagration the weak recuperation regime. It is characterized by monotonic dependencies of $\Theta_{1,2}$ on x. The temperature profiles of core and shell almost merge with slight difference in the reaction zone which is significantly broader than in the case of the strong recuperation regime. This regime of flame propagation is

well described by asymptotic analysis in section 3.3. For the intermediate solution branch, which is not shown here for brevity, the peak value of $Theta_1$ is decreases as we move along the intermediate solution branch from the fast to the slow branch and it disappears for the slow solution branch as shown in figure 4.

It is important to note here that multiple coexisting regimes are also reported for the gas phase combustion in narrow channels with heat recuperation through the solid elements. In [15, 16] it is proposed to produce the excess enthalpy by introducing the highly conductive porous solid into the flame zone. For finite length of the porous solid it was demonstrated that there is a critical flow rate above which the flame quenches and below this critical value two different solutions exist. These solutions are characterized by different temperature of the porous solid and the thickness of the flame zone. In [17, 18] it is demonstrated both experimentally and analytically that for the flame propagating in a gas mixture flowing inside of the narrow channel with walls of the finite thickness multiple regimes of combustion are possible. There are either two or three co-existing combustion waves with different flame velocities and temperatures. The flame multiplicity reported here is a solid fuel analog of the same phenomena in gas mixture combustion with recuperation of heat.

4.2 Stability of combustion waves

In figure 5 the numerical results for flame stability and speed are summarized. The solid lines represent the isocurves of constant speed $u_f = 1$, 2, 3 and 3.8 plotted in s vs. ξ plane for $\alpha = 10^2$, $\beta = 8$ and $\gamma = 0.7$. The s and ξ axes are log-scaled. The neutral stability boundary is shown in figure 5 with the dotted line. Stable combustion wave solutions correspond to the parameter values located inside of the closed loop formed by the dotted curve. The onset of instability is due to the Andronov-Hopf bifurcation thus the curve is marked as 'A-H'. The isocurve $u_f = 1$ marks the boundary in the parameter space: below this curve the flame speed is less than 1 and therefore the composite material is not effective since it burns at the rates slower than the pure energetic material. The heat recirculation subsystem is not working and acts as a thermostat extracting heat from the reacting mixture. Above this curve the flame front propagates faster in composite material than in pure combustible mixture due to the realization of the 'excess enthalpy' concept. The isoline $u_f = 2$ does not form a closed loop in the s-ξ plane either. In the direction of increasing ξ values the conditions for the asymptotic approximations (15) and (24) are met. Thus the speed of combustion wave becomes independent of ξ and isocontours $u_f = 1$ and $u_f = 2$ approach the horizontal lines as seen in figure 5. In the limit $\xi \gg 1$ the velocities as high as $u_f = 3$ cannot be attained and the isocontours for $u_f > 2$ form closed loops in the s-ξ plane. The maximum flame speed possible for the chosen parameter values is slightly larger than 3.8 and the isocurve $u_f = 3.8$ substantially shrinks in area.

There are two particularities in figure 5 worth further consideration. Firstly, it is seen that the neutral stability boundary and isocontours of the combustion front velocity intersect i.e. the faster propagation does not necessarily imply stabilization of deflagration. It should be noted here that in the case of single reacting mixture without recuperation element the travelling combustion wave is unstable for the parameter values considered here. More details on stability analysis can be found in [7]. The other important detail is that the curves $u_f = const$ can intersect as it is seen in figure 5 near the point $s \sim \xi \sim 1$. This is caused by the double folding of the u_f dependence on parameters and multiplicity of solutions as shown in figure 2.

In figure 6 the neutral stability boundary is plotted in s vs. ξ plane for $\alpha = 10^2$, $\gamma = 0.7$ and different values of β equal to 7, 8, 9 and 9.8 shown with the solid, the dash-doted, the dotted and the dashed lines, respectively. For $\beta = 7$ the solid line divides the parameter plane s vs. ξ into two half planes. The stable solutions correspond to parameter values above this curve. Combustion wave for pure energetic material is stable in this case. Therefore, if s is large and the system (5-7) tends to single-step reaction model, the travelling wave solutions of the system (5-7) are stable. For moderate values of s the heat recuperation leads to the flame velocities, $u_f > 1$, larger than in pure energetic material as shown in figure 2. This also stabilizes the combustion wave. As s is decreased the heat recuperation becomes less effective and causes the loss of stability of combustion wave solution. In the limit of small s the model tends to the one-step nonadiabatic case, the core element starts to act as a heat sink or thermostat, the value of $u_f \to 0$ and flame propagation is unstable for all values of ξ.

For the cases of $\beta \geq 8$ the propagation of travelling combustion wave in pure energetic material is unstable. The stabilization of flame propagation is possible in the regions of parameters, where the flame speed is substantially larger than one. These regions occupy compact areas of elliptic shape in the $s - \xi$ parameter plane as it is illustrated in figure 5. In the case $\beta = 8$ the flame is stable inside of the closed contour shown with the dash-dotted line. The flame speed vary from $u_f \approx 1.5$ in the left part of the neutral stability curve to $u_f \approx 3.5$ for the right part of it. For $\beta = 9$ and 9.8 the parameter regions for the stable travelling combustion wave decrease in area and for $\beta \sim 10$ the regime of stable stationary flame propagation disappears.

The nature of multiplicity is further delineated in figure 7, where the flame speed is shown as function of ξ for $\alpha = 10^2$, $s = 1.6$, $\beta = 8$, $\gamma = 0.7$. There are two Andronov-Hopf bifurcations occurring at $\xi \approx 1.29 \times 10^{-2}$ and $\xi \approx 1.65$ which are depicted with diamonds and marked as 'A-H1' and 'A-H2', respectively. Stable travelling wave solutions are found for ξ between these two critical values. There are three distinct branches of solutions: the fast, the slow and the intermediate branches separated by the pair of fold bifurcations marked as 'TP1' and 'TP2'.

Thus we see that the emergence of multiplicity is due to the competition of two flame propagation regimes with strong and weak recuperation of heat. The critical parameter values for the emergence of multiple combustion waves are shown in figure 8, where the solid lines demonstrate the critical parameter values for fold bifurcations in the $s - \xi$ plane for $\alpha = 10^2$, $\beta = 8$, $\gamma = 0.7$. The solid line marked as 'TP1' corresponds to the fold bifurcation from fast to intermediate solution branches. The dashed-dotted line labeled 'TP2' shows the critical parameter values for the onset of the fold bifurcation connecting intermediate and slow solution branches. The neutral stability boundary which is due to the Andronov-Hopf bifurcation is also plotted with the dotted line. The dashed line indicates the choice of parameters in the figure 7. The region of coexistence of triple solutions is located between the curves 'TP1' and 'TP2'.

It is remarkable that in the limit of small values of s the turning point 'TP2' disappears as seen in figure 8, while the other turning point 'TP1' stays at finite values of ξ. Therefore, the dependence of the flame speed on parameters changes from S-shaped depicted in figure 7 to C-shaped function which is typical for the nonadiabatic one-step model. This qualitatively agrees with the analysis in section 3.2.

5 Discussion and Conclusions

In this paper we consider the propagation of deflagration wave in solid composite energetic material of the shell-core type. It is assumed that the heat is conducted according to Fourier's law and the thermal-diffusional approximation is adopted.

It is found that there are two modes of flame propagation is such composite media: the regime of strong and weak recuperation. In the weak recuperation regime the temperatures of shell and core are monotonic functions of coordinate. The distribution of temperature in the inert heat conducting core closely matches the temperature profile of the reacting material in shell with a slight difference in temperatures in the reaction zone. Flame propagates in the composite media as prescribed by one-step reaction adiabatic model with mixed properties: the chemistry of mixture is defined by the reacting energetic material and the thermal diffusivity is governed by the heat conductive core material. According to standard scaling of flame speed it is proportional to the square root of thermal diffusivity of the reacting media [19]. However, the thermal diffusivity of composite material is mostly defined by core material and thus the normal flame speed is proportional to $\alpha^{1/2}$ as shown in figure 1.

In the regime of strong recuperation, the temperature of the core is also monotonic function of coordinate, however the distribution of temperature in reacting shell is characterized by a sharp peak in the reaction zone, which significantly exceeds the adiabatic flame temperature of the pure energetic material. It is remarkable that the temperature profiles of the shell and core of the composite differ substantially i.e. the composite behaves not like a single media with certain properties as in the previous case of weak recuperation regime, but as complex of interacting subsystems: the heat is released in the reacting shell, it is then absorbed from the reaction and product regions by the core and transfered to the fresh mixture. In other words the core serves as a enthalpy feedback loop mechanism and the concept of superadiabatic combustion and excess enthalpy is realized in this regime.

We also found that at certain parameter values when heat capacities of shell and core per unit length in the direction of flame propagation become comparable i.e. $s \sim 1$ the competition of the two flame propagation regimes may lead to the emergence of triple coexisting solutions, propagating with various flame velocities. This is a region of parameters where complex dynamical regimes such as flame hysteresis [14] can be expected to occur and we plan to investigate these scenarios in future work.

From practical point of view the regime of strong recuperation is most desirable, since it delivers the ability to accelerate flame more effectively than by a factor of $\alpha^{1/2}$ as in the case of weak recuperation. Therefore in this paper we are mainly focused on it. It is demonstrated that for the range of parameters considered here the flame speed can be increased by more than the order in magnitude as compared to pure reacting material. Also the increase in flame velocity is accompanied by stabilization of combustion wave. Therefore the strategy of constructing of composite shell-core material can be a very effective way to intensify and stabilize the combustion wave propagation in solid propellants.

In this paper we consider the one-dimensional formulation of the problem. Typically the multi-dimensional combustion wave patterns emerge if the transverse length scale of the system is larger than $\mathcal{D}_T/S_L$, where $\mathcal{D}_T$ and S_L are the thermal diffusivity and the velocity of the planar flame, respectively. Such cases are studied in [20] for cylindrical geometry. The analysis of the present paper is applicable to the systems with transverse width significantly smaller than $\mathcal{D}_T/S_L$. In future work we plan to consider the models where this restriction is omitted and the two- and three-dimensional structures can be formed.

6 Acknowledgements

V.V. Gubernov, A.V. Kolobov would like to acknowledge the financial support from the Russian Foundation for Basic Research grant 13-03-00282.

References

[1] S. Verma and P. Ramakrishna, *Activated charcoal A novel burn rate enhancer of aluminized composite propellants*, Combustion and Flame 157 (2010), pp. 1202 – 1210.

[2] A.S. Rogachev and A.S. Mukasyan Izd. M.: FIZMATLIT Moscow, 2012.

[3] W. Choi, S. Hong, J.T. Abrahamson, J.H. Han, C. Song, N. Nair, S. Baik, and M.S. Strano, *Chemically driven carbon-nanotube-guided thermopower waves*, Nature materials 9 (2010), pp. 423–429.

[4] S. Walia, R. Weber, S. Balendhran, D. Yao, J.T. Abrahamson, S. Zhuiykov, M. Bhaskaran, S. Sriram, M.S. Strano, and K. Kalantar-zadeh, *ZnO based thermopower wave sources*, Chemical Communications 48 (2012), pp. 7462–7464.

[5] S.A. Lloyd and F.J. Weinberg, *A burner for mixtures of very low heat content*, Nature 251 (1974), pp. 47–49.

[6] N. Bakhman and I. Lobanov, *Influence of heat-conducting elements on the burning rate*, Fizika Goreniia i Vzryva 11 (1975), pp. 501–506.

[7] V.V. Gubernov, V.N. Kurdyumov, and A.V. Kolobov, *Flame propagation in a composite solid energetic material*, Combustion and Flame (2014).

[8] Y. Ju and K. Maruta, *Microscale combustion: Technology development and fundamental research*, Progress in Energy and Combustion Science 37 (2011), pp. 669–715.

[9] J.T. Abrahamson, N. Nair, and M.S. Strano, *Modelling the increase in anisotropic reaction rates in metal nanoparticle oxidation using carbon nanotubes as thermal conduits*, Nanotechnology 19 (2008), p. 195701.

[10] C. Yu, L. Shi, Z. Yao, D. Li, and A. Majumdar, *Thermal conductance and thermopower of an individual single-wall carbon nanotube*, Nano Letters 5 (2005), pp. 1842–1846.

[11] G. Joulin and P. Clavin, *Linear stability analysis of nonadiabatic flames: Diffusional-thermal model*, Combustion and Flame 35 (1979), pp. 139 – 153.

[12] J.W. Evans, *Nerve axon equations: III Stability of the nerve impulses*, Indiana Univ. Math. J. 22 (1972), pp. 577–594.

[13] V.V. Gubernov, G.N. Mercer, H.S. Sidhu, and R.O. Weber, *Evans function stability of combustion waves*, SIAM J. Appl. Math. 63 (2003), pp. 1259–1275.

[14] I. Towers, V. Gubernov, A. Kolobov, A. Polezhaev, and H. Sidhu, *Bistability of flame propagation in a model with competing exothermic reactions*, Proceedings of the Royal Society A: Mathematical, Physical and Engineering Science 469 (2013).

[15] T. Takeno and K. Sato, *An excess enthalpy flame theory*, Combustion Science and Technology 20 (1979), pp. 73–84.

[16] T. Takeno, K. Sato, and K. Hase, *A theoretical study on an excess enthalpy flame*, in *Symposium (International) on Combustion*, Vol. 18, 1981, pp. 465–472.

[17] V. Zamashchikov, *Experimental investigation of gas combustion regimes in narrow tubes*, Combustion and Flame 108 (1997), pp. 357–359.

[18] V. Zamashchikov and S. Minaev, *Limits of flame propagation in a narrow channel with gas filtration*, Combustion, Explosion and Shock Waves 37 (2001), pp. 21–29.

[19] G. Sivashinsky, *On the structure and stability of laminar flames*, Annals of the New York Academy of Sciences 404 (1983), pp. 210–214.

[20] T.P. Ivleva, *Propagation of a One-Spot Spinning Wave in a Thick-Walled Cylinder under Adiabatic Conditions*, Combustion, Explosion, and Shock Waves 42 (2006), pp. 403–410.

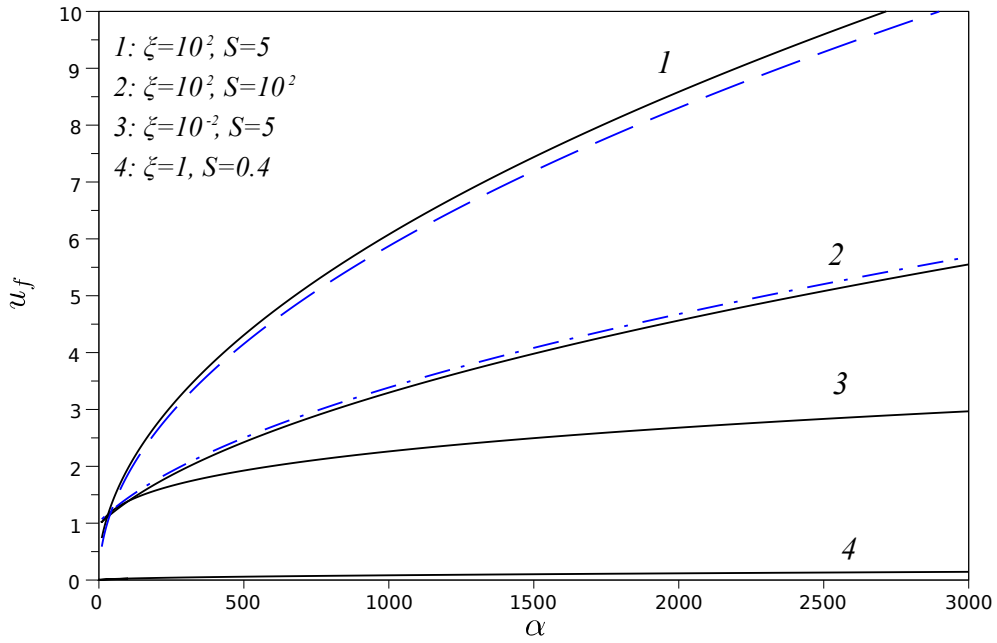

Figure 1: Flame speed, u_f as a function of α for $\beta = 8$ and $\gamma = 0.7$. The solid curves represent the results of numerical calculation for $\xi = 10^2,\ S = 5$ (curve '1'), $\xi = 10^2,\ S = 10^2$ (curve '2'), $\xi = 10^{-2},\ S = 5$ (curve '3'), $\xi = 1,\ S = 0.4$ (curve '4'). The dashed line is plotted according to (24) for $\xi = 10^2,\ S = 5$, while the dash-dotted line shows the dependence (15) for $\xi = 10^2,\ S = 10^2$.

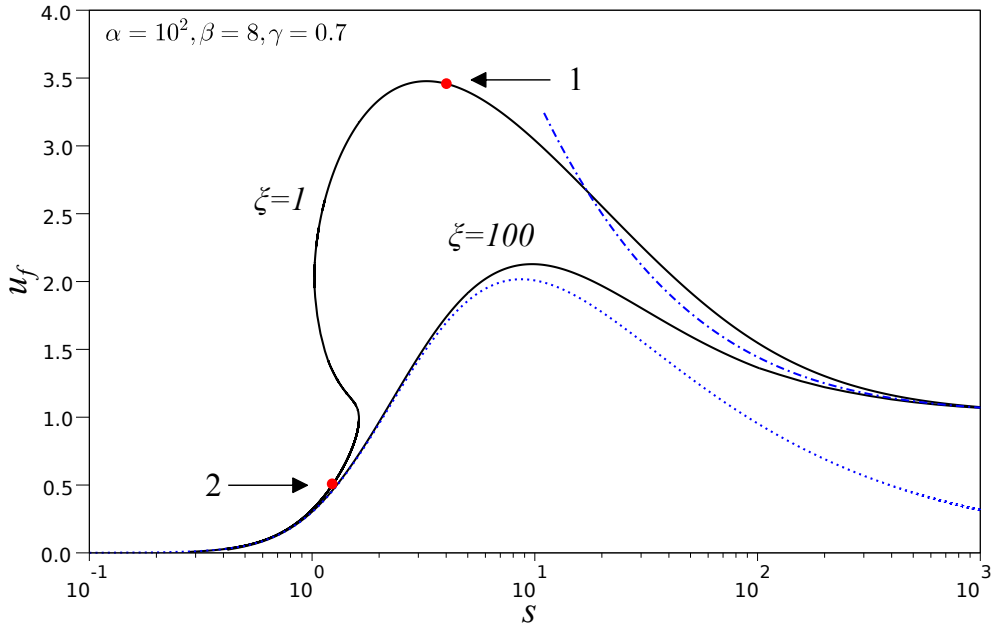

Figure 2: Flame speed as a function of s for $\alpha = 10^2$, $\beta = 8$, $\gamma = 0.7$ and two values of $\xi = 1$ and 10^2. Parameter s is plotted in logarithmic scale. The dash-dotted and the dotted lines represent the asymptotic results (15) and (24), respectively, for the case $\xi = 10^2$.

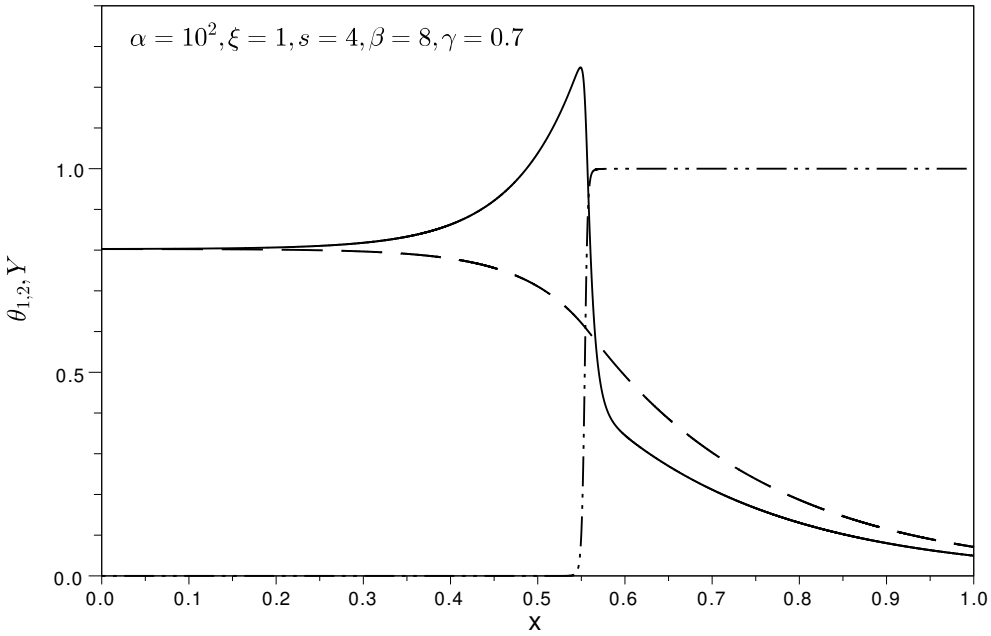

Figure 3: The strong recuperation regime. The temperature $\Theta_1(x)$ (solid line), $\Theta_2(x)$ (dashed line) and mass fraction $Y(x)$ (dash-dotted line) profiles of the travelling combustion wave for $\alpha = 10^2$, $\beta = 8$, $\gamma = 0.7$, $\xi = 1$ and $s = 4$.

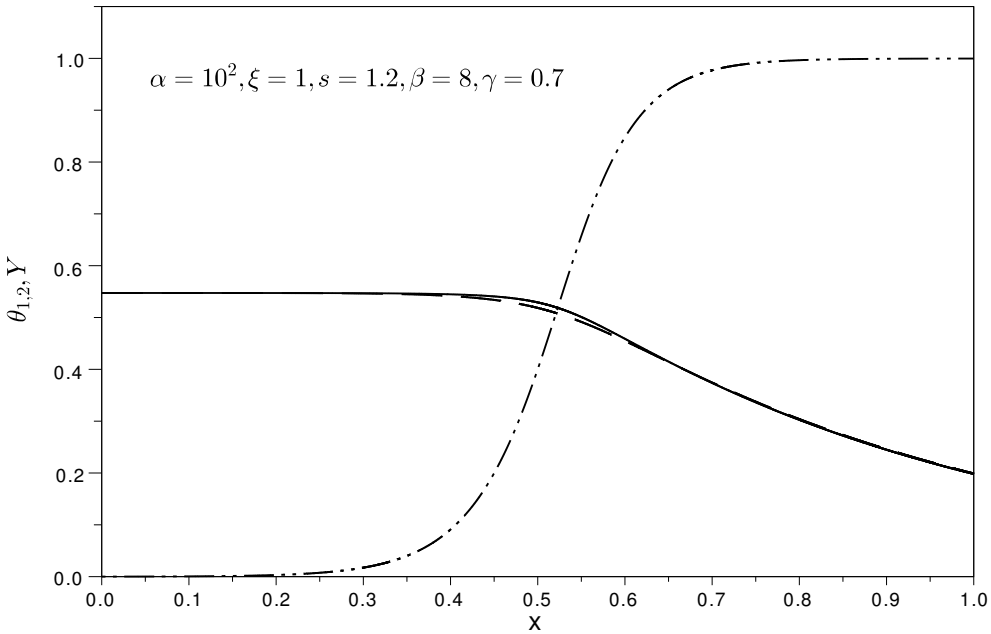

Figure 4: The weak recuperation regime. The temperature $\Theta_1(x)$ (solid line), $\Theta_2(x)$ (dashed line) and mass fraction $Y(x)$ (dash-dotted line) profiles of the travelling combustion wave for $\alpha = 10^2$, $\beta = 8$, $\gamma = 0.7$, $\xi = 1$ and $s = 1.2$.

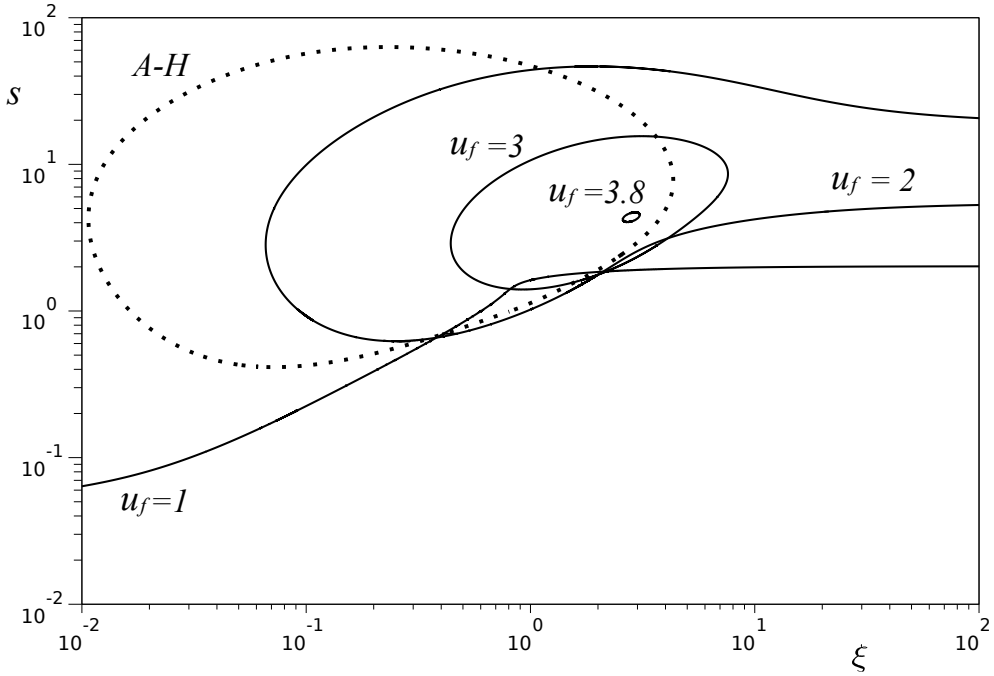

Figure 5: Contours of flame speed $u_f = 1$, 2, 3 and 3.8 on s vs. ξ parameter plane for $\beta = 8$, $\gamma = 0.7$ (the solid lines). Parameters s and ξ are plotted in logarithmic scale. The dashed line represents the critical parameter values for the Andronov-Hopf bifurcation.

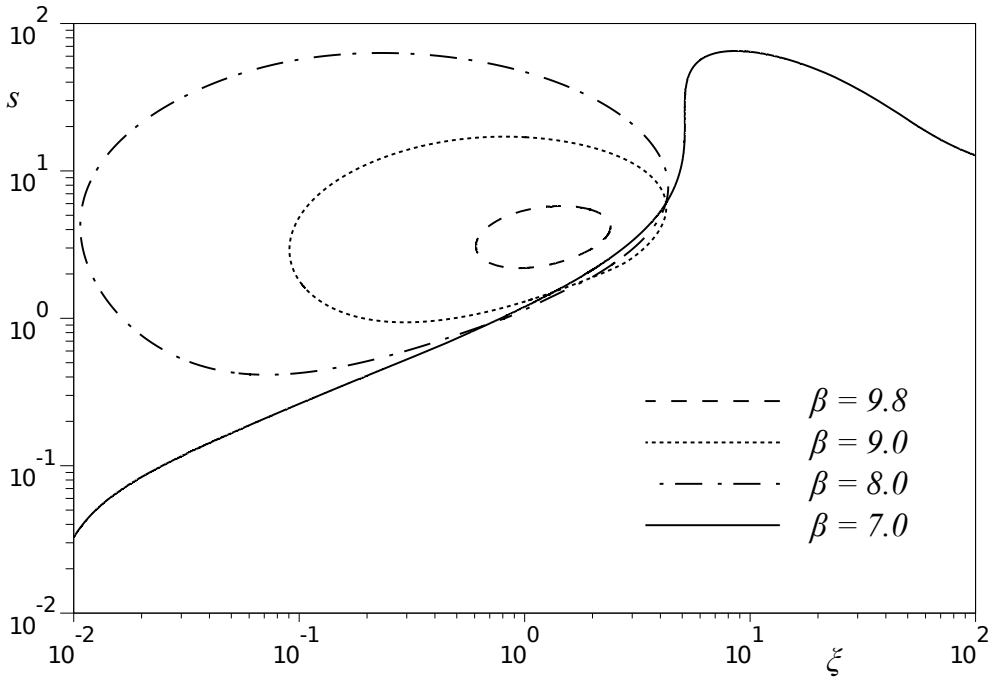

Figure 6: Critical parameter values for the Andronov-Hopf bifurcation in s vs. ξ parameter plane for $\alpha = 10^2$, $\gamma = 0.7$, $\beta = 7$ (solid line), $\beta = 8$ (dash-doted line), $\beta = 9$ (dotted line), and $\beta = 9,8$ (dashed line).

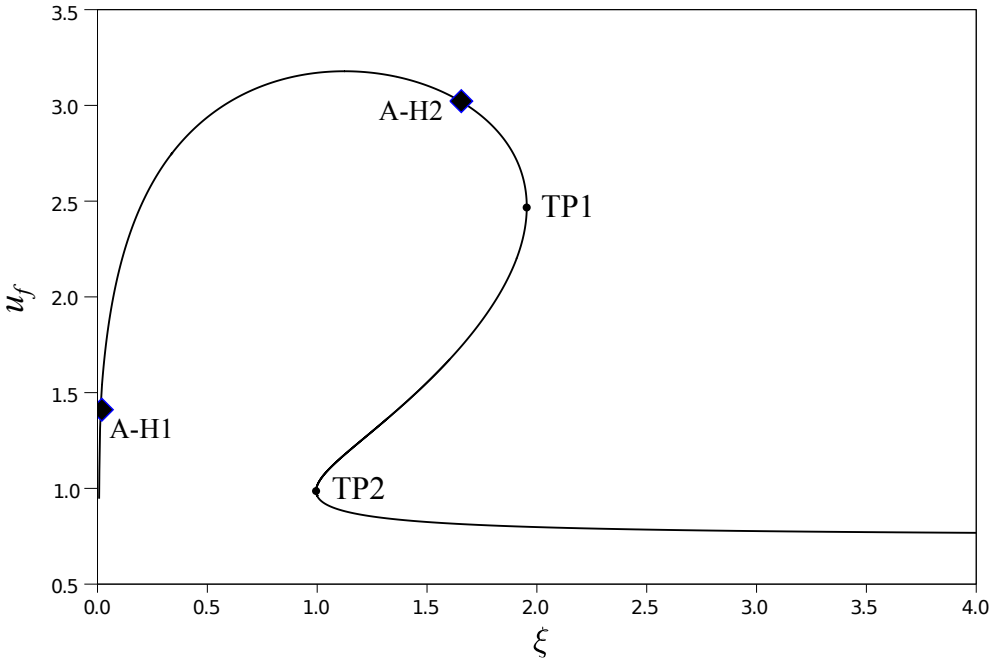

Figure 7: Flame speed as a function of ξ for $\alpha = 10^2$, $\beta = 8$, $\gamma = 0.7$ and $s = 1.6$. The diamonds show the critical parameter values for the Andronov-Hopf bifurcation.

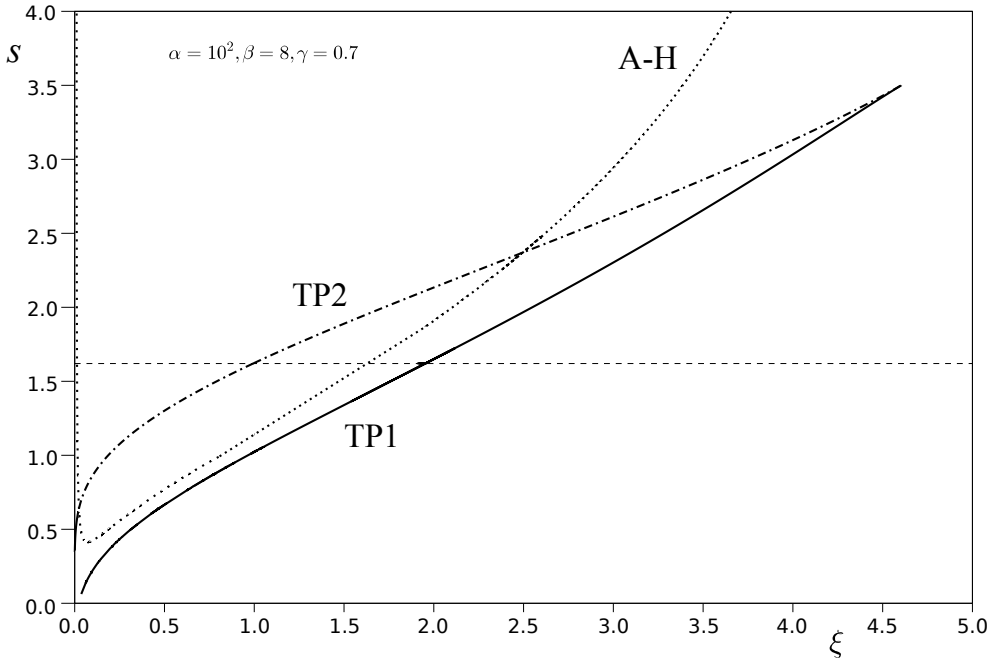

Figure 8: Critical parameter values for the fold ('TP1' and 'TP2') and Andronov-Hopf ('A-H') bifurcations in s vs. ξ parameter plane for $\alpha = 10^2$, $\beta = 8$, $\gamma = 0.7$. The dashed line corresponds to the choice of $s = 1.6$ shown in figure 7.